OPEN ACCESS
IOP Publishing
Plasma Sources Science and Technology
Plasma Sources Sci. Technol. **28** (2019) 115020 (13pp)
https://doi.org/10.1088/1361-6595/ab54e8

Time-resolved optical emission spectroscopy of a unipolar and a bipolar pulsed magnetron sputtering discharge in an argon/oxygen gas mixture with a cobalt target

R Hippler[1,2], **M Cada**[1], **V Stranak**[1] and **Z Hubicka**[1]

[1] Institute of Physics, Czech Academy of Sciences, Na Slovance 2, 18221 Prague, Czech Republic
[2] Institut für Physik, Universität Greifswald, Felix-Hausdorff-Str. 6, D-17489 Greifswald, Germany

E-mail: hippler@physik.uni-greifswald.de

Received 11 June 2019, revised 25 October 2019
Accepted for publication 6 November 2019
Published 28 November 2019

Abstract

Reactive high power impulse magnetron sputtering (HiPIMS) of a cobalt cathode in pure argon gas and with different oxygen admixtures was investigated by time-resolved optical emission spectroscopy (OES) and time-integrated energy-resolved mass spectrometry. The HiPIMS discharge was operated with a bipolar pulsed power supply capable of providing a large negative voltage with a typical pulse width of 100 μs followed by a long positive pulse with a pulse width of about 350 μs. The HiPIMS plasma in pure argon is dominated by Co^+ ions. With the addition of oxygen, O^+ ions become the second most prominent positive ion species. OES reveals the presence of Ar I, Co I, O I, and Ar II emission lines. The transition from an Ar^+ to a Co^+ ion sputtering discharge is inferred from time-resolved OES. The enhanced intensity of excited Ar^{+*} ions is explained by simultaneous excitation and ionisation induced by energetic secondary electrons from the cathode. The intensity of *violet* Ar I lines is drastically reduced during HiPIMS. Intensity of *near-infrared* Ar I lines resumes during the positive pulse indicating an additional heating mechanism.

Keywords: magnetron sputtering, HiPIMS, bipolar pulse, time-resolved optical emission spectroscopy, ion mass spectrometry

1. Introduction

Plasma-based processing techniques are frequently used for applications in fundamental and applied research [1]. Magnetron sputtering is a common technique for deposition of thin solid films [2–4]. Magnetron sputtering can be engaged in different discharge modes, in particular, as direct current (DC), radiofrequency, or pulsed discharge. High power impulse magnetron sputtering (HiPIMS) has attracted much attention in previous years [5–8]. HiPIMS utilises short pulse durations and low repetition rates and, hence, allows for large plasma densities, high ionisation fractions, and large ion fluxes to a substrate [8–12]. A more recent implementation concerns the use of a positive pulse during the afterglow. Nakano *et al* investigated the influence of a positive cathode bias following the negative discharge pulse during the plasma off-time [13]. Bipolar pulsing with a negative discharge pulse followed by positive pulse was utilised by Wu *et al* [14]. Time resolved optical diagnostics and energy-resolved mass spectrometry have revealed details of the ion kinetics [15–17]. A positive pulse enhances the kinetic energy of plasma ions

and provides further process control during film deposition. Bipolar pulsing can give rise to smooth surfaces, dense microstructures, reduces tensile stress, increases hardness and changes the crystallographic orientation of deposited films [15, 17, 18]. Both increased and reduced deposition rates have been reported thus far and a clear picture regarding this aspect has not emerged yet [14, 18].

In the present paper we examine the properties of a HiPIMS plasma with a cobalt cathode for deposition of cobalt oxide films. The influence of a positive pulse following the main (negative) discharge pulse was investigated. Time-resolved optical emission spectroscopy (OES) and energy-resolved mass spectrometry was employed for plasma characterisation. Cobalt is a ferromagnetic metal; it requires a strong magnetic field and a comparatively thin target material for a more efficient use during magnetron sputtering. Cobalt oxide is a material with many attractive optical, magnetic, spintronic, electrochemical, catalytic, and photocatalytic properties [19–25]. Cobalt oxide crystallises as rock salt-type CoO and cubic spinel-type Co_3O_4. Film properties and composition strongly depend on deposition conditions [26]. Models describing the reactive sputtering process and the dependence on plasma parameters have been developed by Nyberg and Berg and by Depla *et al* [27, 28]. The hysteresis effect during HiPIMS was addressed by Strijckmans *et al* [29]. According to these investigations, the hysteresis effect is much smaller during HiPIMS compared to dc magnetron sputtering (DCMS).

2. Experiment

The experimental set-up has been described in detail before [30–32]. A vacuum chamber is equipped with a planar magnetron (high strength magnetic field version) with a Co target (diameter 50.8 mm, nominal thickness 3 mm, purity 99.95%). Argon (purity 99.999%) and oxygen gas (purity 99.995%) is admitted to the vacuum chamber with the help of two gas flow controller. Typical argon and oxygen flow rates are 18–40 sccm and 0–10 sccm, respectively. The argon pressure is set to $p = 1.0$ Pa with the help of a ultrahigh vacuum gate valve between pump and chamber; the gas pressure is measured with a capacitance vacuum gauge (Pfeiffer Vacuum, CMR 365, full range 11 Pa). The magnetron plasma is operated with the help a DC power supply (Advanced Energy MDX-1 K) operated in voltage regulation mode. Pulsed operation was achieved with the help of a home-built power switch delivering a negative pulse during the discharge [33–36]. A second home-built power switch was used for positive pulsing after the first (negative) pulse. A commercial two-channel arbitrary waveform generator (OWON AG 1022) was employed to set the repetition frequency $f = 100$ Hz and the pulse width $T_n = 100\ \mu$s and $T_p = 350\ \mu$s of both negative and positive pulse, respectively, and to trigger the time-resolved measurements. Voltage and current waveforms were simultaneously recorded using

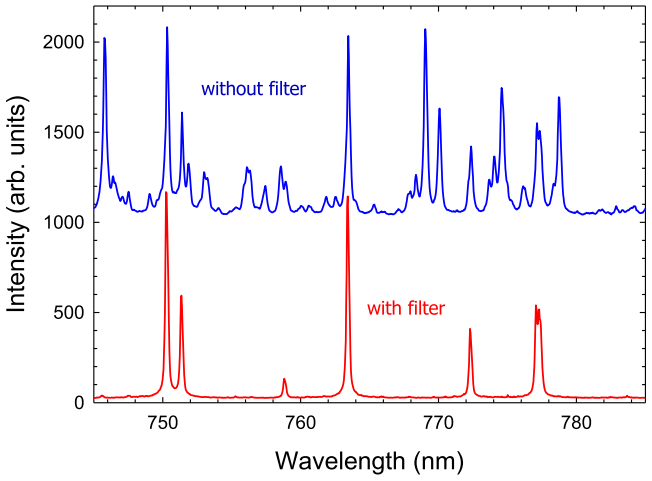

Figure 1. Optical emission spectra in the wavelength range 745–785 nm during HiPIMS. Upper and lower curves show the spectrum obtained without and with filter, respectively. Upper curve shifted upwards by 1000. Ar gas flow 40 sccm, O_2 gas flow 10 sccm, discharge power 150 W.

voltage (Agilent 10076 A) and current probes (Textronix A622) connected to a two-channel digital oscilloscope (Agilent DSO 6012A).

OES was performed with a Shamrock SR500D spectrometer (focal length 500 mm) equipped with an iCCD detector (iStar DH334T-18-U-E3, Andor Technology, Belfast, Northern Ireland). According to the manufacturer's specifications, the quantum efficiency of the photocathode is ≈18% at 400 nm and ≈1.9% at 750 nm. The spectrometer is equipped with three gratings having 600, 1800, and 2400 lines per millimetre. An optical fibre was installed outside the vacuum chamber at an angle of 45° with respect to the target surface; it was connected on the other end to the entrance slit of the spectrometer. A typical slit width was 20 μm. Time-resolved OES measurements are performed with a gate width of 10 μs and with incremental gate steps of 10 μs in the range 0–500 μs. The spectrograph is equipped with a filter wheel in front of the entrance slit. The employed short-pass filter (FESH0800, Thorlabs Inc., Newton, New Jersey, USA) has a high transmission close to 100% in the range 490–800 nm; it is opaque elsewhere. Its purpose is to suppress the second order lines as shown in figure 1. The lower spectrum displays Ar I emission lines with wavelengths in the 750–772 nm range and O I lines at 777.19/777.42/777.54 nm. The upper spectrum additionally displays intense Co I lines in the wavelength range 372–393 nm which appear in second order and are, hence, suppressed in the lower spectrum.

Energy-resolved mass spectrometry is performed with a commercial Hiden EQP 1000 mass/energy analyser (Hiden Analytical Ltd., UK). Further details of the instrument and of the analyzer's settings can be found elsewhere [31, 32]. The instrument is mounted opposite to the magnetron's race track at a distance of 5 cm from the cathode.

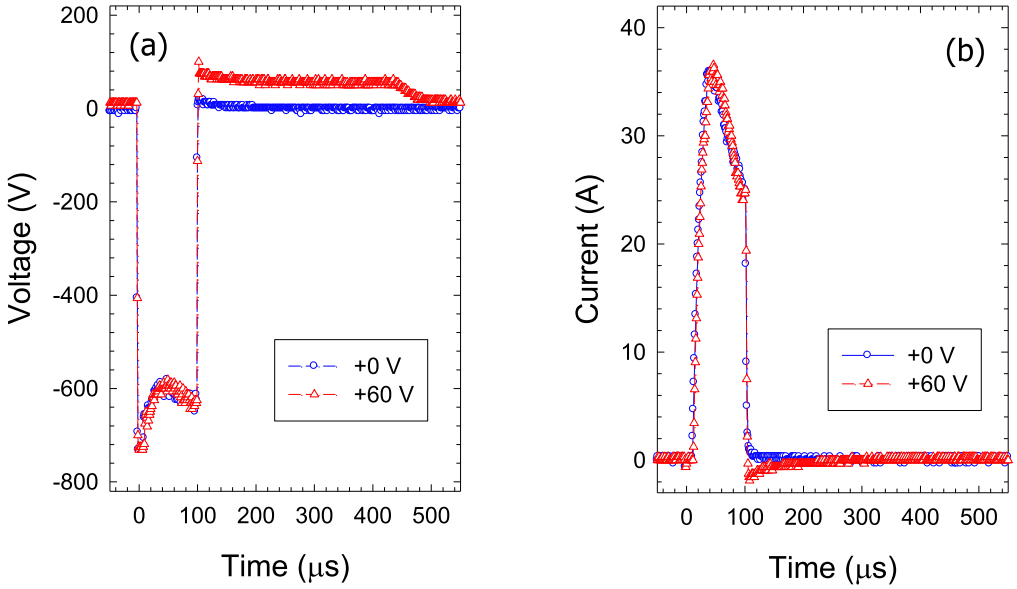

Figure 2. Measured (a) cathode voltage and (b) discharge current as a function of time for a HiPIMS plasma in argon without positive pulse (+0 V, ∘) and with positive pulse (+60 V, △) following the negative pulse. Argon gas flow 40 sccm, gas pressure $p = 1.0$ Pa, discharge power 200 W.

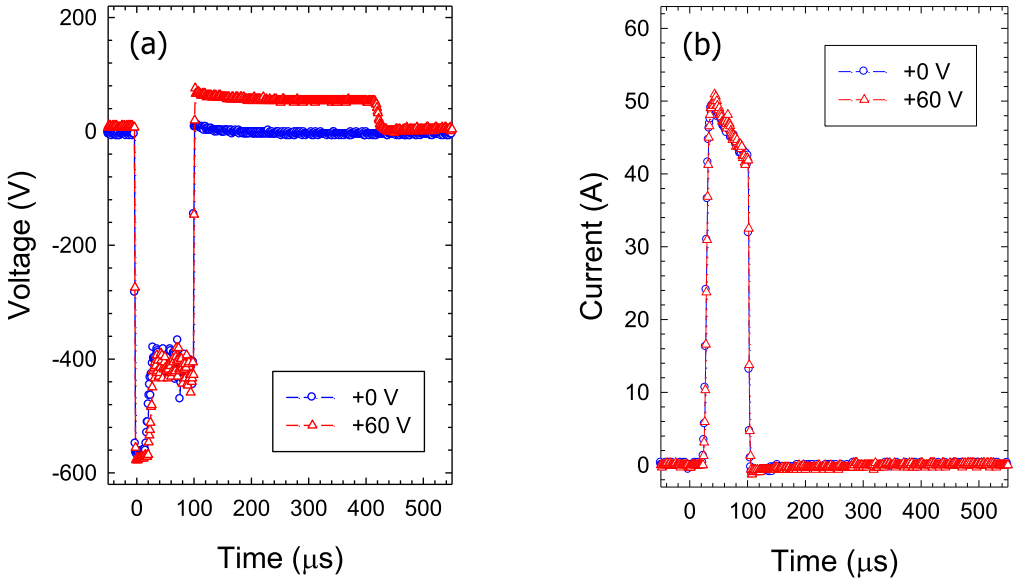

Figure 3. Measured (a) cathode voltage and (b) discharge current as a function of time for a HiPIMS plasma in an argon/oxygen gas mixture without positive pulse (+0 V, ∘) and with positive pulse (+60 V, △) following the negative pulse. Argon gas flow 40 sccm, argon partial gas pressure $p = 1.0$ Pa, oxygen gas flow 10 sccm, discharge power 200 W.

3. Results and discussion

3.1. Current and voltage characteristics

Measured voltage and current waveforms of the magnetron discharge are displayed in figures 2 and 3. Figure 2 shows results for the HiPIMS discharge in pure argon. The voltage applied to the magnetron's cathode drops within 1 μs to -725 V. The voltage remains at this level for about 7 μs prior to its increase to -590 V followed by a slight decrease to about -630 V. The discharge voltage is determined by the impedance of the power supply and of the plasma [37]. The increase marks the ignition of the plasma which is accompanied by an pronounced increase of the discharge current to about 36 A followed by a gradual decrease to 25 A towards the end of the pulse. The decrease of the discharge current after reaching the maximum is attributed to a rarefaction of the working gas. Also shown are the waveforms for the HiPIMS discharge with a positive pulse of +60 V for a duration of about 350 μs following the negative pulse. Due to experimental limitations, there is a small time gap of $\approx$5 μs between negative and positive pulse when the applied voltage is zero. The positive pulse induces a small current of opposite (negative) polarity compared to the regular (positive) discharge current; it rapidly decays with a time constant of

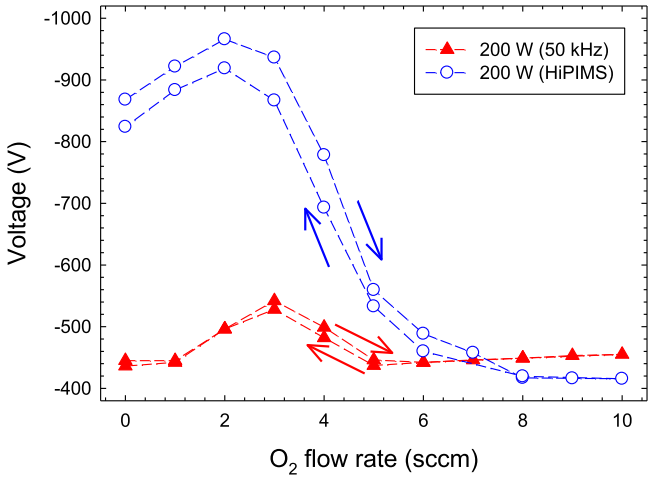

Figure 4. Initial discharge voltage versus O_2 gas flow rate. The magnetron was operated in PMS (50 kHz, ▲) and in HiPIMS (○) mode with a discharge power $P = 200$ W. Argon flow rate 40 sccm, argon pressure $p = 1$ Pa. Arrows indicate increasing/decreasing oxygen gas flow.

≈30 μs. A reversed current with a magnitude of less than 5% of the main discharge current was observed by Britun *et al* during the positive pulse (up to 300 V) of a bipolar HiPIMS discharge [15]. The reversed current displayed two peaks separated in time by 150 μs. The current is presumably formed by negative charge carriers (electrons, negatively charged ions) since the cathode is charged positively. Figure 3 displays voltage and current waveform for the argon/oxygen gas mixture. Major differences compared to the pure argon case are a larger ignition delay of about 20 μs, a smaller ignition voltage of −570 V which increases to −400 V after ignition, and a larger discharge current of 52 A which gradually decreases to 42 A towards the end of the pulse.

The initial discharge voltage versus O_2 gas flow is displayed in figure 4. Without oxygen the required initial discharge voltage is about −870 V. The (negative) voltage decreases to −970 V when oxygen is added to the discharge at a gas flow rate of 2 sccm. Further increasing the gas flow rate results in smaller discharge voltages; the discharge voltage reduces to −415 V at an oxygen flow rate of 10 sccm. For comparison, the initial discharge voltage for pulsed magnetron operation at 50 kHz (duty cycle 60%) is also shown. The observed behaviour can be explained by a variation of the ion-induced secondary electron emission due to the presence of oxygen on the cathode's surface [28, 38]. As indicated in figure 4, the observed oxygen gas flow dependence seems to depend on the direction of the gas flow increase or decrease. The perspectives of a hysteresis during reactive HiPIMS was addressed by Strijckmans *et al* [29]. It has become clear from that investigation that the possibility of a hysteresis, if observed at all, is much smaller during HiPIMS compared to DCMS. A key point concerns the density of free oxygen atoms. Recent studies provide evidence that the O atom density is large during so-called poisoned mode while it is small in so-called metallic mode [39, 40].

3.2. Energy-resolved mass spectrometry

3.2.1. Unipolar regime. Ion energy distributions (IEDs) of plasma ions was investigated by means of energy-resolved mass spectrometry. Figure 5(a) displays energy distributions of Ar^+ and Co^+ ions obtained with a HiPIMS discharge in pure argon. Significant differences in both peak position and energy-integrated intensity are observed between the two ions. The IED of Co^+ has a maximum at ≈12 eV which roughly coincides with the shoulder at ≈11 eV of Ar^+. The IED of Ar^+ ions is dominated by a pronounced maximum at rather small kinetic energies. The energy-integrated intensity of Co^+ is about 40× larger compared to Ar^+ (figure 7). We want to point out that the measured Ar^+ ion intensities are rather small in comparison to previous measurements [32, 41]. There are at least two reasons, in particular, the smaller ionisation probability of Ar compared to Co due to a larger ionisation energy (15.76 eV compared to 7.88 eV, respectively [42]). Secondly, Ar^+ ions are produced by ionisation of thermal gas atoms. Hence, the majority of Ar^+ ions has small kinetic energy, in contrast to Co^+ ions which have received a significantly larger kinetic energy during sputtering. We infer from the rather small Ar^+ ion intensity that a majority of Ar^+ ions is produced in a region with a negative plasma potential which accelerates positive ions towards the cathode. A responsible factor in comparison with previous measurements could be the different magnetic field configuration (high field strength and more balanced) confining electrons closer to the cathode thereby preventing slow ions to escape from that region. We want to emphasise that measured ion intensities and IEDs also show some dependence on the actual target thickness as it influences the magnetic field strength.

Adding oxygen to the HiPIMS discharge (figure 5(b)) leads to a decrease of the energy-integrated intensity of Co^+ ions by approximately one order of magnitude while the Ar^+ ion intensity shows a much weaker decrease. The pronounced decrease of the Co^+ intensity is somewhat compensated by a strong increase of O^+ and O_2^+ ions. Aiempanakit *et al* for an $Ar+O_2$ plasma with a Ti target even observed that O^+ ions have the highest intensity of all ionised species which is in some agreement with our result [43]. The temporal variation of several ion species was investigated by Lundin *et al* using a reactive ionisation region model [40]. Three different (metallic, transition, and poisoned) cathode modes were considered. The model predicts a strong increase of the O^+ density for the poisoned mode which is caused by electron impact ionisation of metastable $O(^3P)$ atoms. The pronounced increase of the O^+ density observed in our experiment agrees well with their result. Energy distributions of O^+ and Co^+ are similar but differ significantly from Ar^+ ions. O^+ ions extend well beyond 100 eV which, in our opinion, suggests that a large fraction of these ions originates from oxygen atoms which are absorbed at the cathode's surface rather than from oxygen atoms and/or molecules in the gas phase. It could also explain the 8× larger intensity of O^+ compared to O_2^+ ions. In addition, we observe a small component of CoO^+

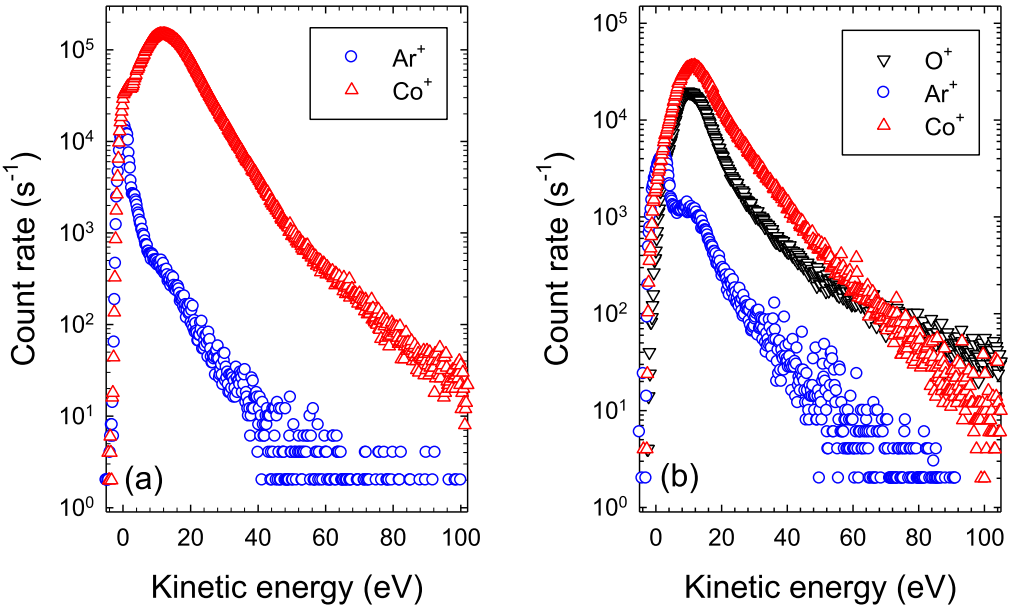

Figure 5. Ion energy distribution of O^+ ($m/z = 16, \triangledown$), Ar^+ ($m/z = 40, \circ$ = open circle) and Co^+ ($m/z = 59, \triangle$) ions of a HiPIMS discharge in (a) pure Ar and (b) in an Ar/O_2 gas mixture. Ar gas flow rate 40 sccm, Ar pressure 1.0 Pa, O_2 gas flow rate 8 sccm, mean discharge power 150 W.

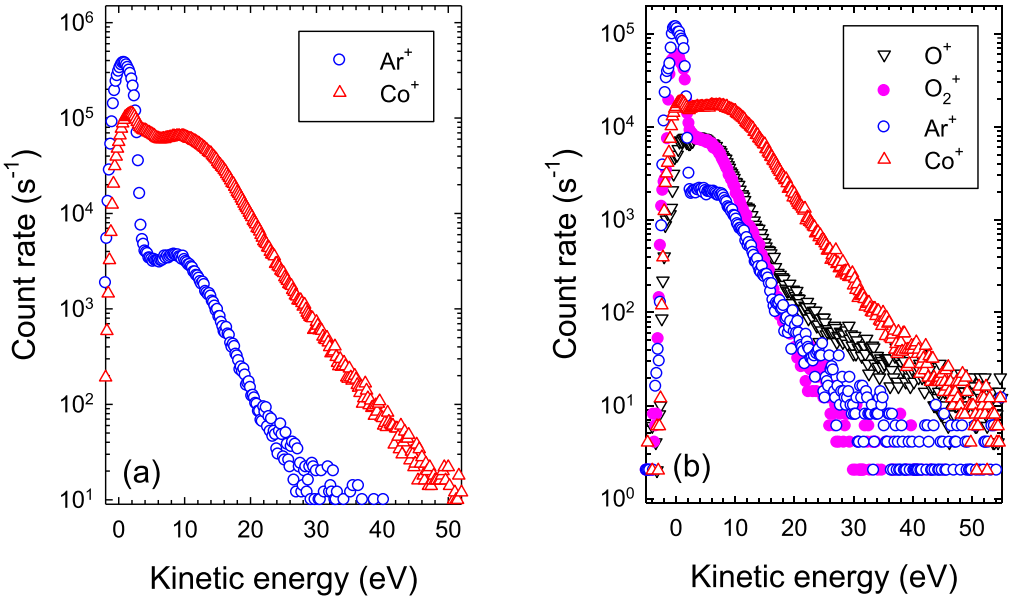

Figure 6. Ion energy distribution of O^+ ($m/z = 16, \triangledown$ = open triangle down), O_2^+ ($\bullet$ = full circle), Ar^+ ($m/z = 40, \circ$ = open circle) and Co^+ ($m/z = 59, \triangle$) ions of a DCMS discharge in (a) pure Ar and (b) in an Ar/O_2 gas mixture. Ar gas flow rate 40 sccm, Ar pressure 1.0 Pa, O_2 gas flow rate 10 sccm, mean discharge power 150 W.

ions which, after an initial increase, displays only a small variation with O_2 gas flow (figure 7).

IEDs of Ar^+ and Co^+ ions during DCMS in pure argon are displayed in figure 6. Both distribution display a more or less pronounced maximum at a small kinetic energy of about 1 eV followed by a second maximum at ≈9 eV which is lower compared to the HiPIMS mode. Measured energy distributions are more narrow in DCMS compared to HiPIMS and hardly extend beyond 40–50 eV.

The measured Co^+ ion intensities without oxygen are one order of magnitude smaller during DCMS compared to HiPIMS which is expected since the ionisation degree during HiPIMS is generally much larger. The opposite holds for Ar^+ ions which are significantly more abundant during DCMS compared to HiPIMS. DCMS requires a smaller cathode potential (figure 4) and, in consequence, a weaker electric field compared to HiPIMS which could further the escape of Ar^+ ions from the electron trap region. With the addition of

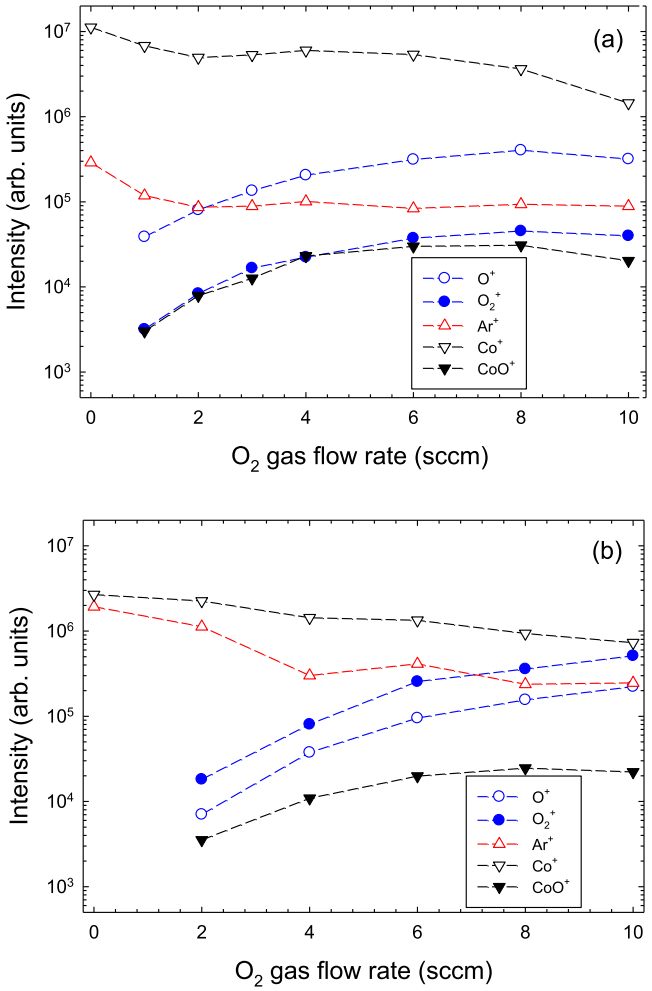

Figure 7. Energy-integrated intensity of O^+ (∘), O_2^+ (•), Ar^+ (△), Co^+ (▽), and CoO^+ (▼ down) ions *versus* O_2 flow rate in an Ar/O_2 gas mixture during (a) HiPIMS and (b) DCMS. Ar gas flow 40 sccm, mean discharge power 150 W.

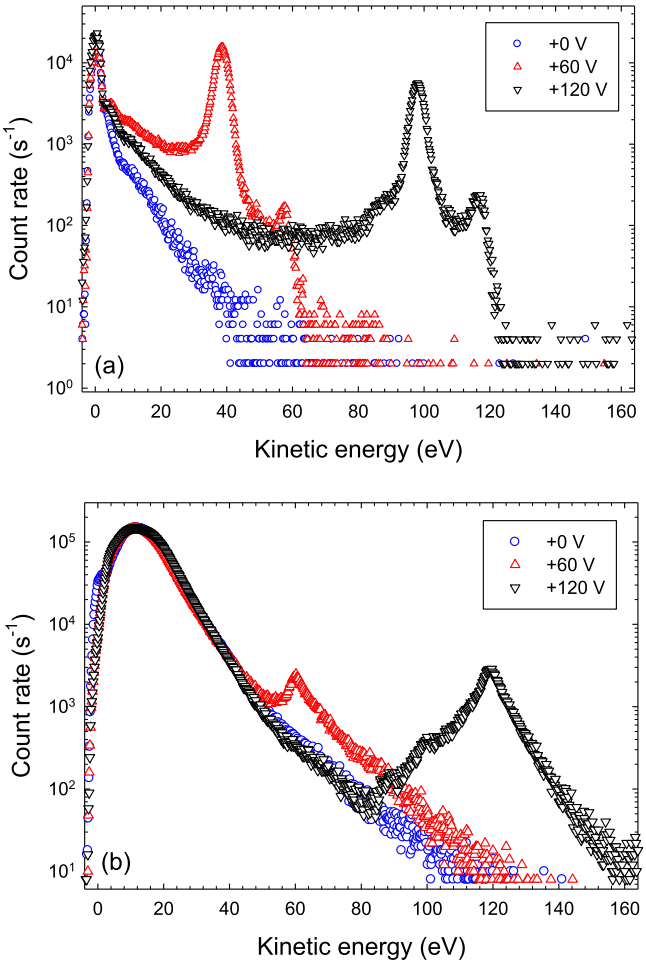

Figure 8. Ion energy distribution of (a) Ar^+ and (b) Co^+ ions in pure Ar of a biploar HiPIMS discharge with a positive pulse of +0 V (∘), +60 V (△), and +120 V (▽). Ar gas flow rate 40 sccm, Ar gas pressure 1.0 Pa, mean discharge power 150 W.

oxygen the intensity of O_2^+ ions strongly increases. Overall, the O_2^+ intensity is 2–3× larger compared to O^+ in the DCMS discharge whereas the opposite was observed during HiPIMS (figure 7). O_2^+ ions are produced in the gas phase and the energy distribution is similar compared to Ar^+ ions.

3.2.2. Bipolar regime. IEDs obtained during bipolar HiPIMS with a positive pulse following the main negative pulse are displayed in figures 8 and 9. Figure 8 displays IEDs of Ar^+ and Co^+ ions in pure Ar with positive pulses of +0 V, +60 V, and +120 V. The Co^+ IED displays an additional peak with a peak energy approximately corresponding to the applied voltage, i.e. at 60 eV and 119 eV for +60 V and +120 V, respectively. The intensity of the additional peaks amounts to about 2%–3% of the main peak at low energies. This is significantly less compared to the results of Keraudy *et al* [16].

The IED of Ar^+ ions differs significantly from that of Co^+ ions. For a positive pulse of +60 V and +120 V a small

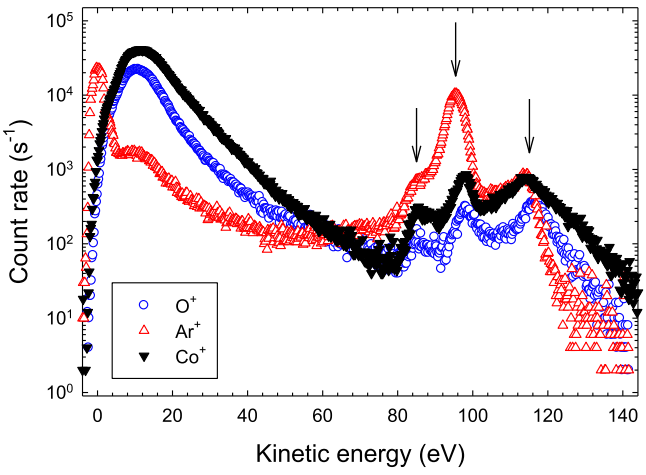

Figure 9. Ion energy distribution of O^+ (∘), Ar^+ (△), and Co^+ (▽) ions in an $Ar+O_2$ gas mixture of a biploar HiPIMS discharge with a positive pulse +120 V. Ar gas flow rate 40 sccm, Ar gas pressure 1.0 Pa, O_2 gas flow rate 10 sccm, mean discharge power 150 W.

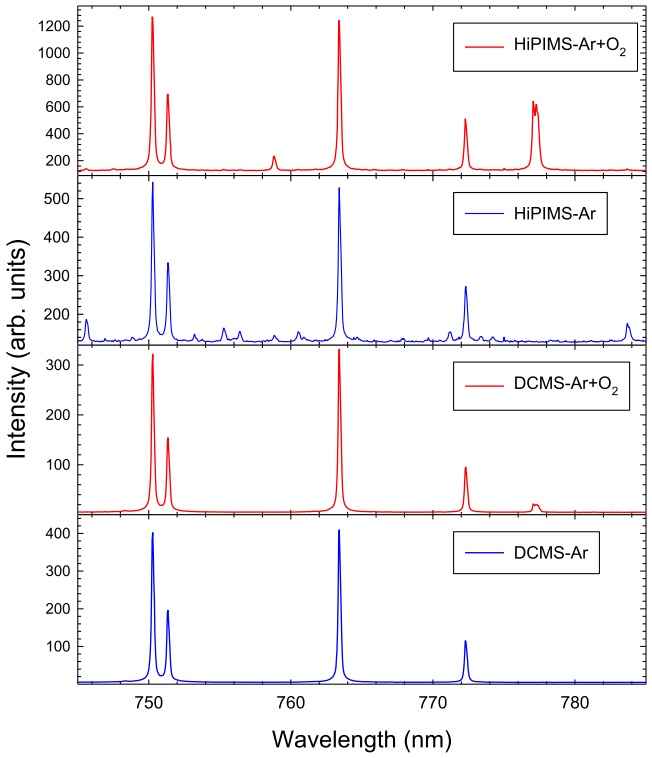

Figure 10. Optical emission spectrum in the wavelength range 745–785 nm obtained in in DCMS and HiPIMS mode in pure Ar (DCMS–Ar, HiPIMS–Ar) and in an Ar+O_2 gas mixture (DCMS–Ar +O_2, HiPIMS–Ar+O_2). Argon gas flow 40 sccm, O_2 gas flow rate 0 sccm (DCMS–Ar, HiPIMS–Ar) and 10 sccm (DCMS–Ar+O_2, HiPIMS–Ar+O_2), argon gas pressure 1.0 Pa, discharge power 150 W.

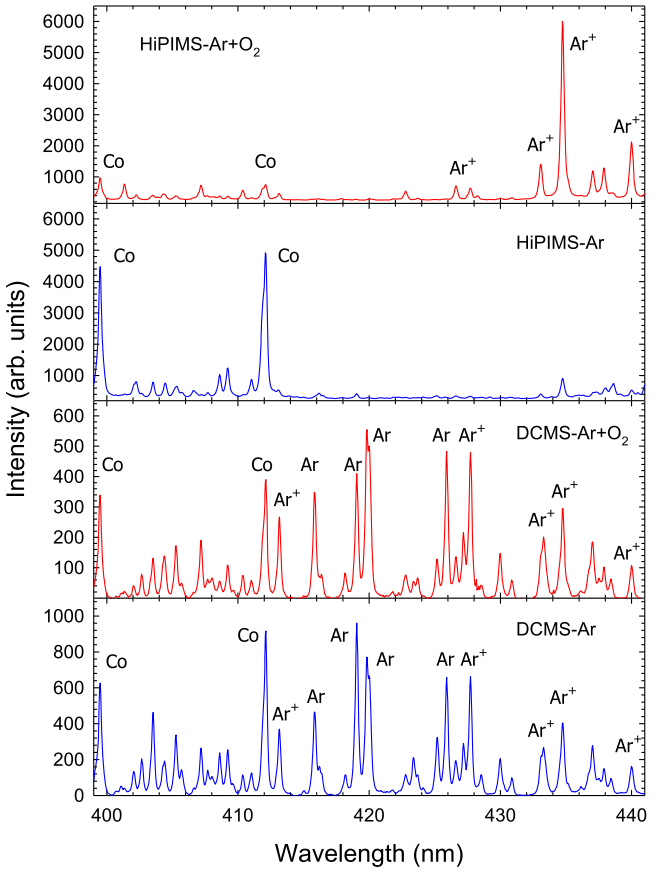

Figure 11. Optical emission spectrum in the wavelength range 399–441 nm obtained in DCMS and HiPIMS mode in pure Ar (DCMS–Ar, HiPIMS–Ar) and in an Ar+O_2 gas mixture (DCMS–Ar +O_2, HiPIMS–Ar+O_2). Argon gas flow 40 sccm, O_2 gas flow rate 0 sccm (DCMS–Ar, HiPIMS–Ar) and 10 sccm (DCMS–Ar+O_2, HiPIMS–Ar+O_2), argon gas pressure 1.0 Pa, discharge power 200 W.

peak which occurs at a somewhat smaller energy of 58 eV and 116 eV, respectively, is observed. The major difference is an orders-of-magnitude larger peak which occurs at a smaller energy of about 38 eV and 98 eV for a positive pulse of +60 V and +120 V, respectively. There are at least two explanations for the additional peak. Ar^+ unlike Co^+ ions are most likely produced in the plasma volume where the electric potential caused by the positive pulse is smaller and thus gives rise to a smaller kinetic energy. Keraudy *et al* based on their observations have proposed a plasma potential profile which extends over several cm from the cathode and essentially remains at the cathode potential over this range [16]; if so, the model will be a variance with our observation. A second interpretation rests on the assumption that the potential in some distance from the cathode is time-dependent which could affect Ar^+ and Co^+ ions in a different way. More experimental investigations will be required to solve this point.

The situation becomes more complicated if oxygen is added to the HiPIMS discharge. Figure 9 displays IEDs of O^+, Ar^+, and Co^+ ions in Ar+O_2 of a bipolar HiPIMS with a positive pulse of +120 V. Observed peaks at about 85 eV, 95 eV, and 115 eV are indicated by arrows. Again, the intensity of the Ar^+ peak at 85 eV is rather strong while other peaks of O^+ and Co^+ ions are much weaker.

3.3. Optical emission spectroscopy

3.3.1. Unipolar regime. Optical emission spectra in the near-infrared (745–785 nm) and in the violet (399–441 nm) spectral range are displayed in figures 10 and 11, respectively. Spectra were taken during DCMS and in HiPIMS mode without oxygen and with oxygen added to the argon gas. Near-infrared emission spectra display the prominent Ar I lines at $\lambda = 750.39$ nm, 751.37 nm, 763.51 nm, and 772.38/772.42 nm which originate from excited Ar(4p) levels with excitation energies in the 13.15–13.48 eV range [42, 44, 45]. The two spectra taken with O_2 added additionally display a O I triplet at 777.19/777.42/777.54 nm which is assigned to $O(3p^5P) \rightarrow O(3s\ ^5S)$ transitions in atomic oxygen [46–48]. All four spectra look fairly alike except for the O I lines which are much stronger in the HiPIMS compared to the DCMS discharge of the Ar+O_2 gas mixture. Intensities of the DCMS spectrum with oxygen admixture are about 3× smaller compared to the pure Ar case, however.

Large differences between the DCMS and HiPIMS modes are noted in the violet part of the OES spectrum (figure 11). Prominent Ar I lines at 415.86 nm, 419.83/420.07 nm, and 425.94 nm, Co I lines at 399.53 nm and

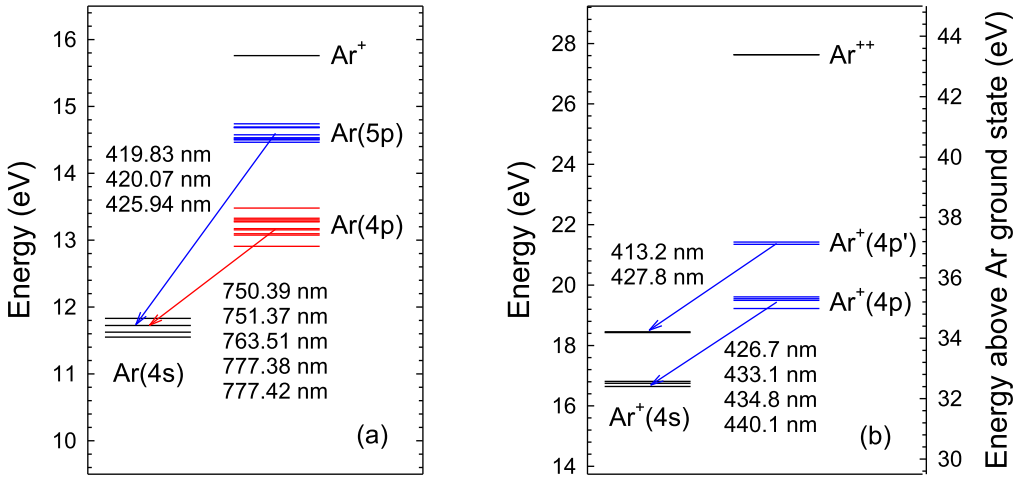

Figure 12. Simplified energy level diagram of (a) Ar I and (b) Ar II [42].

Table 1. Relative intensity of selected Ar I, Ar II, and Co I lines excited by DCMS and HiPIMS in pure Ar (DCMS–Ar, HiPIMS–Ar) and in an Ar+O_2 (DCMS–Ar+O_2, HiPIMS–Ar+O_2) gas mixture. Intensities are normalised to the underlined Ar II intensity. E_{th} excitation energy with respect to the argon ground state [42], σ excitation cross section by electron impact from the argon ground state at an electron energy of 50 eV [65].

	Ar I		Ar II		Co I
Line (nm)	419.8/420.1	425.94	427.8	434.8	411.9/412.1
E_{th}(eV)	14.58/14.50	14.74	37.11	35.25	3.93/4.06
σ (10^{-20} cm^2)	23/10	23	25	33	—
DCMS–Ar	225	138	170	<u>100</u>	166
DCMS–Ar+O_2	164	100	127	72	78
HiPIMS–Ar	8	12	20	<u>100</u>	713
HiPIMS–Ar+O_2	<5	<5	55	811	70

412.13 nm, and Ar II lines at 407.20 nm, 413.17 nm, 427.75 nm, 433.12/433.20 nm, 434.81 nm, 437.08/437.13 nm, and 440.10 nm are observed in the DCMS mode in both, pure Ar and Ar+O_2, gas mixtures [42]. Other strong Co I lines are observed at wavelengths below 400 nm (not shown here). Co I lines originate from excitation of low-lying excited states including the ground state, e.g. Co($3d^7 4s4p$) or Co($3d^8 4p$). The required excitation energies from the ground state are about 4 eV and thus much smaller compared to Ar I and Ar II excitation energies (table 1). Ar I emission lines in this wavelength range originate from Ar(5p) → Ar(4s) transitions with excitation energies in the 14.46–14.74 eV range (figure 12). Observed Ar II lines stem from excitation of $Ar^+(4p\ ^4D°)$ and $Ar^+(4p\ ^4P°)$ quartet or $Ar^+(4p'\ ^2D°)$ and $Ar^+(4p'^2\ P°)$ doublet states. Addition of O_2 to the DCMS discharge reduces the overall line intensity by about 35% but does not change significantly the spectral distribution (table 1).

The violet spectrum taken in HiPIMS mode in pure argon displays strong Co I lines with about one order of magnitude larger intensity compared to DCMS while neutral Ar I lines are virtually absent. The intensity of Co I decreases by one order of magnitude when oxygen is added to the HiPIMS discharge (table 1). The pronounced decrease of the Co I line intensity is readily explained by the decreasing sputtering yield due to cathode poisoning with oxygen [27, 28, 49]; it is supported by the observed order-of-magnitude reduction of the deposition rate measured with a quartz micro balance [50]. The intensity of Ar II lines strongly increases with the addition of oxygen to the HiPIMS discharge in contrast to the DCMS discharge where the intensity slightly decreases. A similar rise of Ar^+ line emission was reported for a HiPIMS discharge with oxidised Nb and Fe cathodes [51, 52].

The time dependence of several Ar I (763.51 nm), Co I (412.10 nm), and Ar II (434.80 nm) lines during the HiPIMS pulse in pure argon is shown in figure 13(a). The Ar I line intensity increases rapidly right after ignition; it is followed by a pronounced decrease towards the end of the pulse. Intensities of Co I and Ar II lines increase significantly slower and remain nearly constant during the entire pulse. It indicates that the initial phase is dominated by excitation (and ionisation) of Ar atoms whereas in the later phase excitation (and ionisation) of sputtered Co atoms becomes dominant. The decreasing Ar I intensity during the pulse is explained by gas rarefaction due to the strong sputtering wind from the cobalt cathode. In addition, a decrease of the electron temperature during the pulse could play a role [53]. The decreasing Ar^+ ion current to the cathode is (partly)

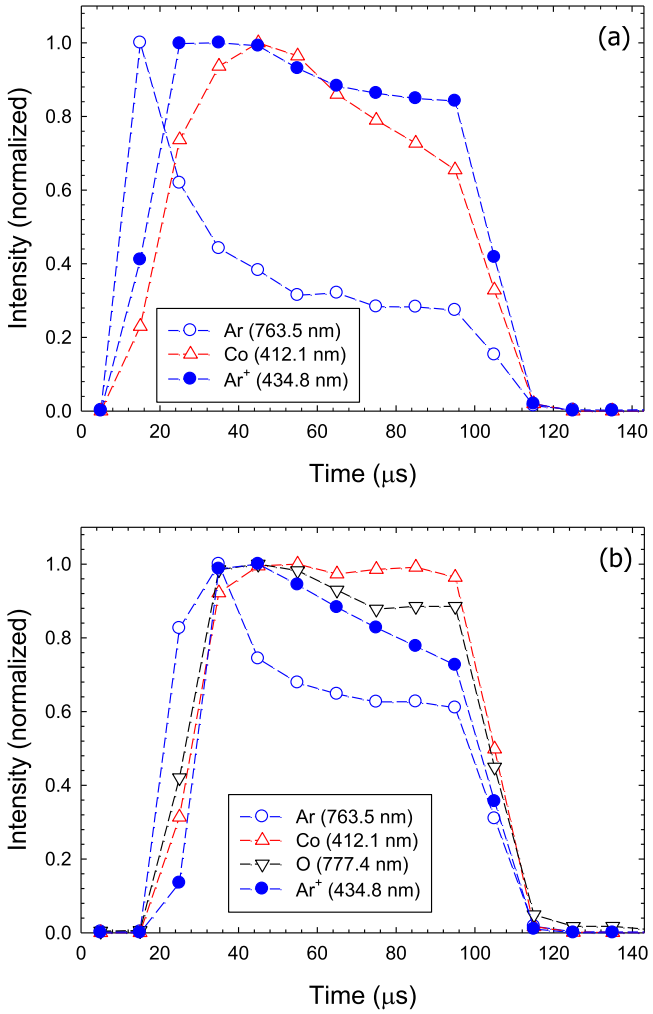

Figure 13. Time dependence of Ar I (763.51 nm, ○), Co I (412.10 nm, △), Ar II (434.80 nm, •), and O I (777.19/777.42/777.54 nm, ▽) lines during HiPIMS in (a) pure Ar and (b) in an Ar/O_2 gas mixture. Discharge power 200 W, Ar gas flow rate 40 sccm, O_2 gas flow rate 10 sccm, argon gas pressure 1.0 Pa.

compensated by Co^+ ions which return to the cathode and give rise to self-sputtering. We would like to emphasise that the sputtering yield of Co by Ar^+ or Co^+ ions is comparatively large, about 1.04 or 1.16, respectively, at 500 eV, which is, e.g. more than twice compared to Ti sputtering [54]. We mention in passing that the Co I line intensity rather closely follows the time dependence of the discharge current (figure 2). Similar observations and conclusions were also noted in other experiments with different target materials [38, 55, 56]. The behaviour of the Ar II ion line is intermediate between the Ar I and Co I lines: the Ar II intensity increases somewhat slower compared to Ar I and faster compared to Co I lines.

Figure 13(b) displays the time dependence of Ar I, Co I, O I, and Ar II line intensities for the $Ar+O_2$ gas mixture. Some differences compared to the pure Ar case are noted, in particular, the larger ignition delay of $\approx 20\,\mu s$ and the less pronounced decrease of the Ar I line intensity by approximately one third after reaching its maximum. The observation indicates that gas rarefaction has become less important due to the reduced sputtering yield caused by cathode poisoning. Co I and O I line intensities remain nearly constant until the end of the pulse while the Ar II line intensity shows a weak decrease.

Several processes can contribute to the formation of excited Ar^{+*} states, in particular, direct excitation of Ar^+ ions by electron (e^-) impact, $e^- + Ar^+ \rightarrow e^- + Ar^{+*}$, and simultaneous excitation and ionisation of argon atoms, $e^- + Ar \rightarrow e^- + Ar^{+*} + e^-$. Direct excitation requires an energy transfer in the range of 19.22–19.64 eV or 21.35–21.50 eV for the $Ar^+(4p)$ or $Ar^+(4p')$ states, respectively, of interest here. Significantly larger is the energy transfer for simultaneous excitation and ionisation which, for the same excited states, requires 34.98–35.40 eV or 37.11–37.26 eV (figure 12). The relative importance of the two processes depends on the energy distribution of electrons, the respective cross sections, and the fraction of Ar^+ ions. The electron energy distribution during magnetron sputtering has at least two components, a (thermalized) low-energy component with typical electron temperatures in the range $T_e \approx 2$–3 eV and $T_e \approx 3$–6 eV for DCMS [57] and HiPIMS [36, 53], respectively, and a high-energy component of energetic secondary electrons from the cathode with kinetic energies of several 100 eV. It has been shown that high-energy electrons constitute a significant fraction of the electron energy distribution function during HiPIMS, in particular, at the beginning of the pulse [53]. Evidence of a high-energy component in DCMS discharges is derived from the measured intensity ratio I_{420}/I_{419} of the 420.07 nm and 419.83 nm Ar I lines. The lines are not resolved in figure 11. However, measurements carried out with a better spectral resolution employing the 1800 lines mm^{-1} grating enables the separation of the two lines and a determination of their relative intensities. We measure an intensity ratio $I_{420}/I_{419} \approx 0.89$ and $I_{420}/I_{419} \approx 0.90$ for the DCMS and DCMS–O_2 discharge, respectively. According to Boffard *et al* [58], a ratio of $I_{420}/I_{419} < 1$ is an indication of a significant high-energy electron component with kinetic energies of more than 25 eV.

The next point to consider is the fraction (ionisation degree) of Ar^+ ions. Typical electron densities in DCMS are a few $10^{16}/m^3$ which corresponds to an ionisation degree of about 10^{-4} (at a gas pressure of 1 Pa) [57]. Corresponding numbers for the HiPIMS discharge are more than $10^{18}/m^3$ and a few 10^{-2} [9, 59]. Moreover, the ionisation degree of a HiPIMS discharge is time-dependent and starts from about zero at the beginning of a pulse. Thus, due to a small ionisation degree, the direct excitation process is rather unlikely and the simultaneous excitation and ionisation processes is expected to dominate.

Cross sections for simultaneous excitation and ionisation of selected Ar II lines (427.75 and 434.81 nm) and for direct excitation of Ar I lines (419.83/420.07 nm and 425.94 nm) are given in table 1 for an electron energy of 50 eV. All cross sections at this particular energy are approximately the same and if we generalise this argument to other electron energies the roughly equal line intensities during DCMS in pure Ar and in the $Ar+O_2$ gas mixture can be explained.

The pronounced increase of the Ar^+ line intensity during HiPIMS with oxygen admixture points to an additional origin. We know from IED measurements that energetic O^+ ions dominate the ionic composition. Hence, interaction of energetic O^+ ions in, for example, charge exchange collisions with Ar atoms

$$O^+ + Ar \rightarrow O + Ar^{+*} \quad (1)$$

which proceed via formation of a transient quasi-molecule [60, 61] could play an important role in this context. Reactions of this type are known for He^+ ions with kinetic energies as low as a few 10 eV which can interact with neutral Ar atoms to form excited Ar^{+*} ions [62, 63].

The disappearance of Ar I lines is explained by de-excitation to energetically close electronic states, for example, Ar(4d) with binding energies of 14.69–15.00 eV, respectively [42]. The violet Ar I lines originate from Ar(5p) → Ar(4s) transitions where the upper Ar(5p) states have binding energies in the range of 14.46–14.74 eV [42]. The density of Ar(5p) states is governed by excitation, de-excitation, and decay rates. The time evolution of the Ar(5p) density n_{5p} may be expressed as

$$\frac{dn_{5p}(t)}{dt} = k_1 n_e n_{Ar} - k_2 n_e n_{5p} - A n_{5p}, \quad (2)$$

where k_1 and k_2 are the rate coefficients for excitation and de-excitation, respectively, of the Ar(5p) state, $A \approx 10^7/s$ [64] is the radiative decay rate, n_{Ar} is the Ar atom density, and n_e is the electron density. Excitation from the argon ground state by electron impact and de-excitation by electron and/or ion impact (ion density $n_+ = n_e$) is assumed. Under equilibrium conditions, we obtain

$$\frac{n_{5p}}{n_{Ar}} = \frac{k_1}{k_2/\alpha + A/\bar{n}_e}, \quad (3)$$

where $\bar{n}_e = \alpha n_e = 10^{16}\,m^{-3}$ and α are time-averaged electron density and duty cycle, respectively, which takes the time-structure and, hence, the temporally enhanced electron density of a pulsed discharge into account. $\alpha = 0.01$ and 1 is the duty cycle of the employed HiPIMS and DCMS discharge, respectively. For a qualitative understanding we include the two limiting cases $k_2 n_e \ll A$ and $k_2 n_e \gg A$ which we expect for the DCMS and HiPIMS discharge, respectively, which holds if k_2 is in the range of 10^{-5}–$10^{-3}\,cm^3\,s^{-1}$. The large value of k_2 compared to k_1 is readily justified by the orders-of-magnitude larger cross section for de-excitation compared to excitation from the ground state and the small fraction of electrons with kinetic energies larger than the excitation energy. Figure 14 shows the relative Ar(5p) density calculated with the help of equation (3) as function of duty cycle for different values of the de-excitation rate coefficient k_2. It is noted that de-excitation can lead to a drastic reduction of the Ar(5p) density and thus can explain the disappearance of the violet Ar I lines. The same mechanisms will also work for Ar(4p) excitation. However, we expect in this case a significantly smaller de-excitation rate which, in combination with a larger excitation rate, should have a minor influence on the observed near-infrared Ar I lines.

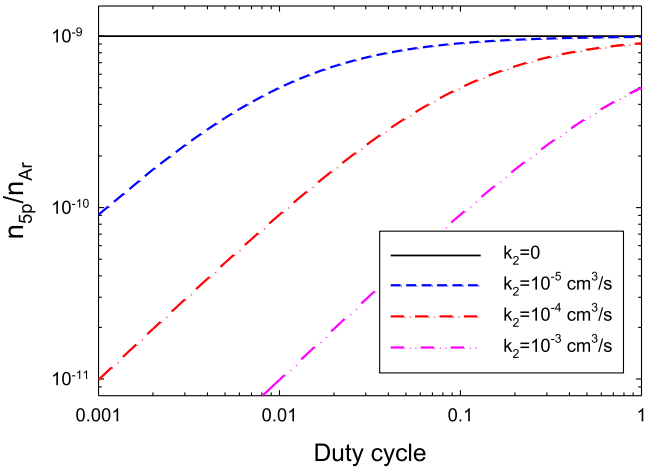

Figure 14. Relative density of Ar(5p) states *versus* duty cycle calculated with the help of equation (3) for a time-averaged electron density $\bar{n}_e = 10^{16}/m^3$ and different rate coefficients k_2 (see text).

3.3.2. Bipolar regime. Time-resolved OES was carried out for bipolar HiPIMS, i.e. with an additional positive pulse after the end of the negative HiPIMS pulse (see figure 2). A positive pulse enhances the kinetic energy of plasma ions by approximately $e\,U_{pos}$ where U_{pos} is the applied positive voltage and e is the (positive) elementary charge [16]. The time dependence of Ar I (763.51 nm), Co I (412.10 nm), and Ar II (434.80 nm) lines during bipolar HiPIMS in pure argon is shown in figure 15(a). The first 100 μs correspond to the *standard* HiPIMS (without positive pulse) and no significant difference between the unipolar and bipolar case is noted in this time interval. Large differences are noted for the time domain with the positive pulse (time $t > 100\,\mu s$), in particular, for the Ar I line intensity. After a short decline which resembles the time gap of ≈5 μs between negative and positive pulse, the Ar I line intensity resumes to a slightly larger value from which it gradually declines until the signal disappears at about 250 μs after the commencement of the positive pulse. It is well known that the electron density in the off phase (afterglow) shows a multi-exponential decay with time constants of ≈40 and ≈210 μs [36, 66]. The electron temperature in the afterglow regime reduces significantly and, as is evident from our results with the unipolar pulse, becomes too small for excitation of atoms or ions [30]. Hence, we propose that the behaviour of the Ar I line during the positive pulse is caused by returning electrons of the expanding plasma produced during the main (negative) pulse which gain kinetic energy by the applied positive voltage. We have also varied the applied voltage during the positive pulse. As shown in (figure 16)(a), a threshold voltage of ≈25 V is required which is about 10 V larger compared to the excitation energy. Co I and Ar II line intensities diminish at the end of the negative pulse and do not resume during the positive pulse. Excitation of Ar II lines by simultaneous

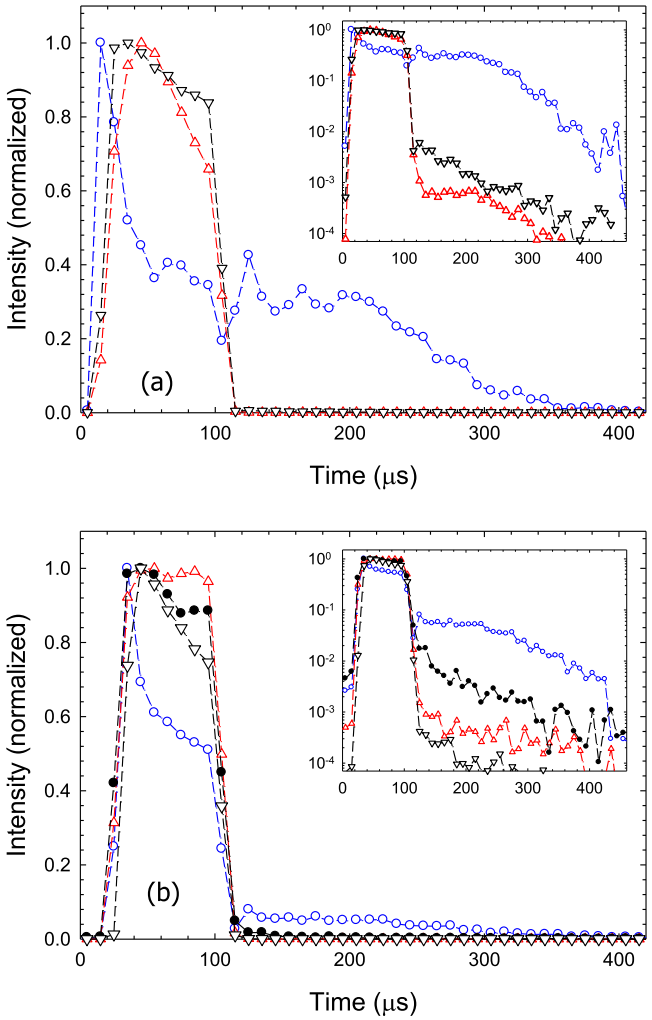

Figure 15. Time dependence of Ar I (763.51 nm, ∘), Co I (412.10 nm, △), Ar II (434.80 nm, ▽), and O I (777.19/777.42/777.53 nm, •) lines during HiPIMS with bipolar pulse (+60 V) in (a) pure Ar and (b) in an Ar/O_2 gas mixture. Discharge power 200 W, Ar gas flow rate 40 sccm, argon gas pressure 1.0 Pa, O_2 gas flow rate 10 sccm.

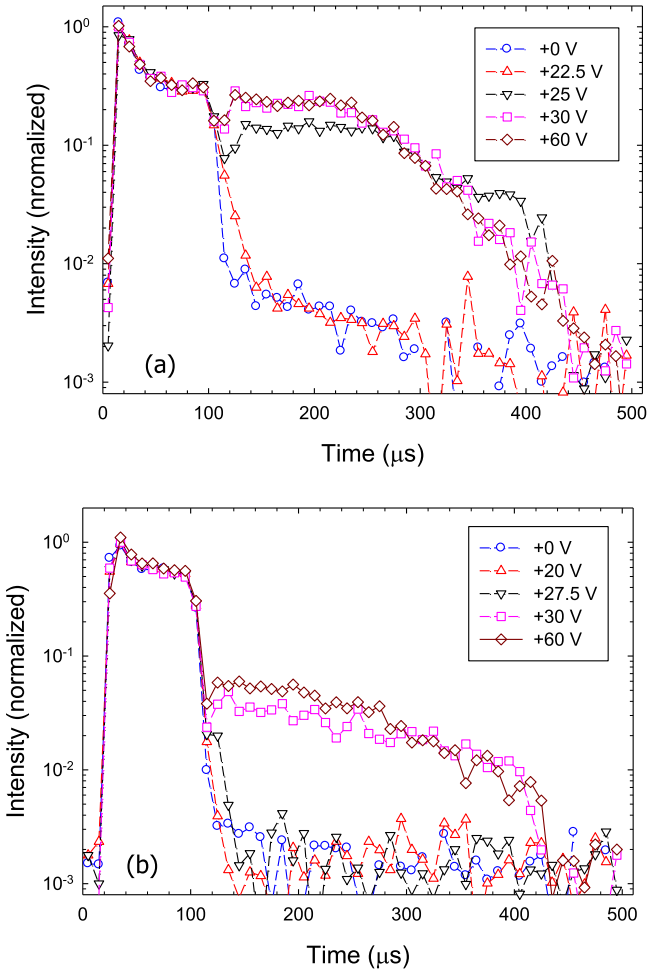

Figure 16. Time dependence of Ar I lines during HiPIMS with bipolar pulse in (a) pure Ar and (b) in an Ar/O_2 gas mixture for the indicated positive voltages. Discharge power 200 W, Ar gas flow rate 40 sccm, argon gas pressure 1.0 Pa, O_2 gas flow rate 10 sccm.

excitation and ionisation of neutral Ar atoms requires about 35–37 eV which may be too large. In addition, we have to take into account that Ar^+ ions are expelled from the cathode region by the positive pulse. Britun *et al* have shown that the intensity of Ti^+ ions decreases by about one order of magnitude within the first 150 μs of the positive pulse [15]. Excitation of Co I lines requires an energy transfer of ≈4 eV only (table 1). However, Co atoms are produced during the negative pulse only and with typical energies in the 10 eV range. It takes less than 10 μs for a 10 eV Co atom to travel a distance of 5 cm and only a few Co atoms should be present near the cathode region during the positive pulse. Figure 15(b) displays the time dependence of Ar I, O I, Co I, and Ar II line intensities during bipolar HiPIMS with an $Ar+O_2$ gas mixture. Noted differences to the pure Ar case are a significantly reduced Ar I line intensity during the positive pulse. Even weaker is the intensity of the O I line intensity during the positive pulse while Co I and Ar II line intensities have diminished. The observation supports our hypothesis of a returning accelerated electron cloud as the electron density in Ar/O_2 is smaller compared to the pure Ar case [36]. The required minimum voltage is about +30 V and thus 5 V larger compared to the pure Ar case (figure 16(b)).

4. Conclusions

Reactive HiPIMS of a cobalt cathode in pure argon gas and with different oxygen admixtures was investigated by OES and energy-resolved mass spectrometry. The HiPIMS discharge was operated in unipolar mode with a negative voltage and in bipolar mode with an additional positive pulse following the negative pulse. The unipolar HiPIMS plasma in pure argon is dominated by Co^+ ions; the intensity of Ar^+ ions is comparatively small. O^+ intensity strongly increases with increasing oxygen gas flow. It is attributed to an oxidised cathode. IED measurements with bipolar pulsing reveal the appearance of a new peak at an energy corresponding to the applied voltage. The intensity of this new peak amounts to a few percent of the main peak. For Ar^+ ions a second and

much stronger peak appears at a kinetic energy which is about 23–25 eV smaller than the first peak. The exact origin of this peak is not clear yet and will require further investigations. OES shows strong Ar I, Co I, O I, and Ar II line emissions. The near-infrared part of the OES spectrum is dominated by Ar I lines resulting from excitation of Ar(4p) states. The disappearance of Ar I lines in the violet spectral range is explained by quenching of Ar(5p) states by de-excitation processes which increase with plasma density. The enhanced intensity of excited Ar^{+*} lines is explained by simultaneous excitation and ionisation of ground state Ar atoms induced by energetic secondary electrons from the cathode. Time-resolved OES reveals a change from an Ar-dominated to a Co-dominated discharge within the first 20 μs. Light intensity diminishes at the end of the unipolar (negative) pulse. The intensity of Ar I lines resumes during bipolar HiPIMS when a positive pulse is applied. Co I and Ar I lines do not show an enhancement in this time domain. It is explained by returning electrons which gain energy by the applied positive voltage. It does not affect the Co I lines as sputtering has ceased and Co atoms are no longer produced.

Acknowledgments

The work was partly supported by project no. 19-00579S of the Czech Science Foundation, by project no. FV30177 of the Ministry of Industry and Trade of the Czech Republic, and by project no. SOLID21-CZ.02.1.01/0.0/0.0/16_019/0000760 of the Operational Programme Research, Development and Education financed by European Structural and Investment Funds and the Czech Ministry of Education, Youth and Sports.

ORCID iDs

R Hippler https://orcid.org/0000-0002-5956-3321
M Cada https://orcid.org/0000-0001-6826-983X
V Stranak https://orcid.org/0000-0001-9676-634X
Z Hubicka https://orcid.org/0000-0002-4051-057X

References

[1] Hippler R *et al* (ed) 2008 *Low Temperature Plasmas* vols 1 and 2 (Berlin: Wiley-VCH)
[2] Waits R K 1978 *J. Vac. Sci. Technol.* **15** 179
[3] Thornton J A 1978 *J. Vac. Sci. Technol.* **15** 171
[4] Ellmer K 2008 *Low Temperature Plasmas* ed H Hippler *et al* (Weinheim: Wiley-VCH Verlag) p 675
[5] Kouznetsov V, Macak K, Schneider J M, Helmersson U and Petrov I 1999 *Surf. Coat. Technol.* **122** 290
[6] Anders A 2011 *Surf. Coat. Technol.* **205** S1
[7] Stranak V *et al* 2009 *J. Phys. D: Appl. Phys.* **42** 105204
[8] Stranak V, Cada M, Hubicka Z, Tichy M and Hippler R 2010 *J. Phys. D: Appl. Phys.* **108** 043305
[9] Gudmundsson J T, Alami J and Helmersson U 2001 *Appl. Phys. Lett.* **78** 3427
[10] Rauch A, Mendelsberg R J, Sanders J M and Anders A 2012 *J. Appl. Phys.* **111** 083302
[11] Anders A, Capek J, Hala M and Martinu L 2012 *J. Phys. D: Appl. Phys.* **45** 012003
[12] Gudmundsson J T, Lundin D, Brenning N, Raadu M A, Huo C and Minea T M 2016 *Plasma Sources Sci. Technol.* **25** 065004
[13] Nakano T, Murata C and Baba S 2010 *Vacuum* **84** 1368
[14] Wu B, Haehnlein I, Shchelkanov I, McLain J, Patel D, Uhlig J, Jurczyk B, Leng Y and Ruzic D N 2018 *Vacuum* **150** 216
[15] Britun N, Michiels M, Godfroid T and Snyders R 2018 *Appl. Phys. Lett.* **112** 234103
[16] Keraudy J, Viloan R P B, Raadu M A, Brenning N, Lundin D and Helmersson U 2019 *Surf. Coat. Technol.* **359** 433
[17] Velicu I-L, Ianos G-T, Porosnicu C, Mihaila I, Burducea I, Velea A, Cristea D, Munteanu D and Tiron V 2019 *Surf. Coat. Technol.* **359** 97
[18] Viloan R P B, Gu J, Boyd R, Keraudy J, Li L and Helmersson U 2019 *Thin Solid Films* **688** 137350
[19] Barakat N A M, Khil M S, Sheikh F A and Kim H Y 2008 *J. Phys. Chem.* C **112** 12225
[20] Chung W S, Yang S M, Kim T W and Hong J P 2016 *Sci. Rep.* **6** 37503
[21] Satoh T, Iida R, Higuchi T, Fujii Y, Koreeda A, Ueda H, Shimura T, Kuroda K, Butrim V I and Ivanov B A 2017 *Nat. Commun.* **8** 638
[22] Shang C, Dong S, Hu P, Guan J, Xiao D, Chen X, Zhang L, Gu L, Cui G and Chen L 2015 *Sci. Rep.* **5** 8335
[23] Jiang Z-J and Jiang Z 2016 *Sci. Rep.* **6** 27081
[24] Liao L *et al* 2014 *Nat. Nanotechnol.* **9** 69
[25] Dvorakova M *et al* 2019 *Catal. Today* **334** 13
[26] Neto N F A, Leite D M G, Lisboa-Filho P N and da Silva J H D 2018 *J. Vacuum Sci. Technol.* A **36** 061512
[27] Berg S and Nyberg T 2005 *Thin Solid Films* **476** 215
[28] Depla D, Heirwegh S, Mahieu S, Haemers J and Gryse R De 2007 *J. Appl. Phys.* **101** 013301
[29] Strijckmans K, Moens F and Depla D 2017 *J. Appl. Phys.* **121** 080901
[30] Sushkov V, Do H T, Cada M, Hubicka Z and Hippler R 2013 *Plasma Sources Sci. Technol.* **22** 015002
[31] Hippler R, Cada M, Stranak V, Hubicka Z and Helm C A 2017 *J. Phys. D: Appl. Phys.* **50** 445205
[32] Hippler R, Cada M, Stranak V, Helm C A and Hubicka Z 2019 *J. Appl. Phys.* **125** 013301
[33] Stranak V, Quaas M, Wulff H, Hubicka Z, Wrehde S, Tichy M and Hippler R 2008 *J. Phys. D: Appl. Phys.* **41** 055202
[34] Stranak V, Hubicka Z, Adamek P, Blazek J, Tichy M, Spatenka P, Hippler R and Wrehde S 2006 *Surf. Coat. Technol.* **201** 2512
[35] Cada M, Adamek P, Stranak V, Kment S, Olejnicek J, Hubicka Z and Hippler R 2013 *Thin Solid Films* **549** 177
[36] Hippler R, Hubicka Z, Cada M, Ksirova P, Wulff H, Helm C A and Stranak V 2017 *J. Appl. Phys.* **121** 171906
[37] Helmersson U, Lattemann M, Bohlmark J, Ehiasarian A P and Gudmundsson J T 2006 *Thin Solid Films* **513** 1
[38] Keraudy J, Delfour-Peyrethon B, Ferrec A, Garcia Molleja J, Richard-Plouet M, Payen C, Hamon J, Corraze B, Goullet A and Jouan P-Y 2017 *J. Appl. Phys.* **121** 171916
[39] Britun N, Konstantinidis S, Belosludtsev A, Silva T and Snyders R 2017 *J. Appl. Phys.* **121** 171905
[40] Lundin D, Gudmundsson J T, Brenning N, Raadu M A and Minea T M 2017 *J. Appl. Phys.* **121** 171917
[41] Hippler R, Cada M, Stranak V and Hubicka Z 2019 *J. Phys. Commun.* **3** 055011
[42] Kramida A, Ralchenko Yu, Reader J and NIST ASD Team 2015 *NIST Atomic Spectra Database (ver. 5.3)* (Gaithersburg, MD: NationalInstitute of Standards and Technology) http://physics.nist.gov/asd (12 May, 2017)

[43] Aiempanakit M, Aijaz A, Lundin D, Helmersson U and Kubart T 2013 *J. Appl. Phys.* **113** 133302
[44] Sushkov V P, Do H T and Hippler R 2013 *Contrib. Plasma Phys.* **53** 549
[45] Sushkov V, Herrendorf A-P and Hippler R 2016 *J. Phys. D: Appl. Phys.* **49** 425201
[46] Smirnov V V, Stelmakh O M, Fabelinsky V I, Kozlov D N, Starik A M and Titova N S 2008 *J. Phys. D: Appl. Phys.* **41** 192001
[47] Wildt J, Fink E H, Biggs P and Wayne R P 1989 *Chem. Phys.* **139** 401
[48] Wildt J, Fink E H, Biggs P, Wayne R P and Vilesov A F 1992 *Chem. Phys.* **159** 127
[49] Wolter M, Do H T, Steffen H and Hippler R 2005 *J. Phys. D: Appl. Phys.* **38** 2390
[50] Hubicka Z 2019 private communication
[51] Hala M, Capek J, Zabeida O, Klemberg-Sapieha J E and Martinu L 2012 *J. Phys. D: Appl. Phys.* **45** 055204
[52] Stranak V, Hubicka Z, Cada M, Bogdanowicz R, Wulff H, Helm C A and Hippler R 2018 *J. Phys. D: Appl. Phys.* **51** 095205
[53] Poolcharuansin P and Bradley J W 2010 *Plasma Sources Sci. Technol.* **19** 025010
[54] Matsunami N, Yamamura Y, Itikawa Y, Itoh N, Kazumata Y, Miyagawa S, Morita K, Shimizu R and Tawara H 1983 *Energy Dependence of the Yields of Ion-Induced Sputtering of Monatomic Solids, IPPJ-AM-32* (Japan: Institute of Plasma Physics, Nagoya University)
[55] Oks E and Anders A 2009 *J. Appl. Phys.* **105** 093304
[56] Britun N, Konstantinidis S and Snyders R 2015 *Plasma Process. Polym.* **12** 1010
[57] Hippler R, Wrehde S, Stranak V, Zhigalov O, Steffen H, Tichy M, Quaas M and Wulff H 2005 *Contrib. Plasma Phys.* **45** 348
[58] Boffard J B, Wang S, Lin C C and Wendt A E 2015 *Plasma Sources Sci. Technol.* **24** 065005
[59] Cada M, Hubicka Z, Adamek P, Kluson J and Jastrabik L 2011 *Surf. Coat. Technol.* **205** S317
[60] Wille U and Hippler R 1986 *Phys. Rep.* **132** 129
[61] Toepfer A, Gross E K U and Dreizler R M 1980 *Z. Phys.* A **298** 167
[62] Lipeles M, Novick R and Tolk N 1965 *Phys. Rev. Lett.* **15** 815
[63] Lipeles M 1971 *Phys. Rev.* A **4** 140
[64] Inoue G, Setser D W and Sadeghi N 1982 *J. Chem. Phys.* **76** 977
[65] Boffard J B, Chiaro B, Weber T and Lin C C 2007 *At. Data Nucl. Data Tables* **93** 831
[66] Bowes M and Bradley J W 2014 *J. Phys. D: Appl. Phys.* **47** 265202